

Chemical Evolution of Dwarf Spheroidal and Blue Compact Galaxies

Gustavo A. Lanfranchi^{1,2} and Francesca Matteucci²

¹*IAG-USP, R. do Matão 1226, Cidade Universitária, 05508-900 São Paulo, SP, Brazil*

²*Dipartimento di Astronomia-Università di Trieste, Via G. B. Tiepolo 11, 34131 Trieste, Italy*

1 November 2018

ABSTRACT

We studied the star formation and chemical evolution in a sample of 8 Dwarf Spheroidal (dSph) galaxies of the Local Group and in Blue Compact Galaxies (BCGs) by means of comparison between the predictions of chemical evolution models and several observed abundance ratios. Detailed models with up to date nucleosynthesis taking into account the role played by supernovae of different types (II, Ia) were developed for both types of galaxies allowing us to follow the evolution of several chemical elements (H, D, He, C, N, O, Mg, Si, S, Ca, and Fe). The models are specified by the prescriptions of the star formation and galactic wind efficiencies chosen to reproduce the main features of these galaxies. The BCGs are characterized by a star formation proceeding in several short bursts separated by long quiescent periods and by a low wind efficiency, whereas one or two long bursts and a very efficient wind well describe the dSph galaxies. We also investigated a possible connection in the evolution of dSph and BCGs and compared the predictions of the models to the abundance ratios observed in Damped Lyman α Systems (DLAs). The main conclusions are: i) the observed distribution of $[\alpha/\text{Fe}]$ vs. $[\text{Fe}/\text{H}]$ in dSph galaxies is mainly a result of the star formation rate coupled with the wind efficiency; ii) a low star formation efficiency ($\nu = 0.01 - 1 \text{ Gyr}^{-1}$) and a high wind efficiency ($w_i \sim 5 - 15$) are required to reproduce the observational data for dSph galaxies; iii) the low gas content of these galaxies is the result of the combined action of gas consumption by star formation and gas removal by galactic winds; iv) the BCGs abundance ratios are reproduced by models with 2 to 7 bursts of star formation and an efficiency in the range $\nu = 0.1 - 0.9 \text{ Gyr}^{-1}$; v) the low values of N/O observed in BCGs are the natural result of a bursting star formation; vi) a connection between dSph and BCGs in an unified evolutionary scenario is unlikely; vii) the models for both the dSph galaxies and BCGs reproduce the abundance ratios observed in DLAs, but imply different formation scenarios for these objects; viii) a suitable amount of primary N produced in massive stars can be perhaps an explanation for the low plateau in the $[\text{N}/\alpha]$ distribution observed in DLAs, if real.

Key words: galaxies: abundances – galaxies: Local Group – galaxies: evolution – galaxies: high-redshift – quasars: general

1 INTRODUCTION

The Dwarf Spheroidal galaxies are important objects to understand the formation and evolution of galaxies. They could be the building blocks for the assembly of the larger galaxies in the scenario of hierarchical structure formation and contribute to improve our knowledge of the nucleosynthesis of the elements. Understanding their star formation (SF) and chemical enrichment histories can help in clarifying these issues. If the Local Group dSph galaxies are indeed the small structures from which the halo of our Galaxy was formed, one should see a similarity between the patterns of the abun-

dance ratios observed in the halo stars and in the dSph galaxies. Besides that, the determination of the abundances and abundance ratios of several elements in these galaxies offers an unique opportunity to improve our knowledge on the formation of the elements.

Recently, the dSph galaxies have been the subject of a great deal of studies concerning accurate abundance determination with high dispersion spectroscopy allowing a detailed study of their star formation and chemical enrichment histories (Shetrone, Bolte & Stetson 1998; Smecker-Hane & McWilliam 1999; Bonifacio et al. 2000; Shetrone, Coté & Sargent 2001; Shetrone et al. 2003; Tolstoy et al.

2003). Shetrone et al. (2003), using UVES spectra of 15 individual red giants in 4 dSph galaxies of the Local Group, measured the abundances of a series of elements including α and iron-peak ones. They showed that the dSph giants exhibit α/Fe ratios lower than those observed in the metal-poor Galactic halo in the same abundance range, as already noticed by Shetrone, Coté & Sargent (2001). They suggested that the low abundance ratios at low metallicities could be due to a slow star formation rate (SFR), which was also suggested by Tolstoy et al. (2003) for the same galaxies. Tolstoy et al. (2003) also noticed that the dSph galaxies of the Local Group exhibit similar abundance patterns suggesting a fairly uniform chemical evolution, despite their different star formation histories.

The star formation histories of dSph galaxies of the Local Group were inferred by means of color magnitude diagrams (CMDs). These galaxies show a wide range of different star formation histories with some systems showing signs of extended or bursting periods of star formation while others are consistent with just one burst in the early epochs of the evolution of the galaxy (Smecker-Hane 1997; Smecker-Hane & McWilliam 1999; Hernandez, Gilmore & Valls-Gabaud 2000; Dolphin 2002). These differences in the star formation histories should be visible also in the pattern of the observed abundance ratios, especially of those elements which are produced on different time-scales, such as the α and iron-peak elements, respectively. Thus, the comparison of key abundance ratios with predictions of chemical evolution models allows one to constrain the effects of star formation episodes and different star formation histories.

Models for dSph galaxies using star formation histories and the observed $[\text{Mg}/\text{Fe}]$ as observational constraints were proposed recently in the literature (Carraro et al. 2001; Carigi, Hernandez & Gilmore 2002; Ikuta & Arimoto 2002). Ikuta & Arimoto (2002) used a chemical evolution model coupled with a simulation code for CMD in order to calculate the star formation and chemical enrichment histories considering the effects of the chemical evolution on photometric properties. They concluded that the observed $[\text{Mg}/\text{Fe}]$ ratios and the morphologies of the observed CMDs of local dSph galaxies can be reproduced by a star formation with long duration ($> 3.9 - 6.5$ Gyr) and very low rates ($10^{-2} - 5 \cdot 10^{-3}$ Gyr^{-1}). In a different approach, Carigi, Hernandez & Gilmore (2002) used star formation histories inferred by CMDs as a constraint to obtain information on the history of parameters of galactic evolution such as gas infall, outflows and global metallicities of local dSph galaxies. Carraro et al. (2001) using N-body/hydro-dynamical simulations including star formation, supernova (SN) feed-back and chemical evolution suggested that there is an ample possibility for the star formation history in these galaxies, ranging from a single short initial episode to longer ones, burst-like activities and very prolonged star formation in agreement with what is suggested by CMDs. In their simulations the gas content is removed from the luminous part of the galaxy by galactic winds.

The galactic wind, in fact, might be a very important feature in the evolution of the dSph galaxies since these are very gas-poor systems. Indeed, in many of these galaxies no interstellar medium (ISM) was detected and upper limits on the ratio between HI and total mass are around 0.004 (Mateo 1998). However, the mechanism responsible for the removal

of the gas content of these galaxies is not known and some assumptions such as gas stripping by our Galaxy (Ikuta & Arimoto 2002) or winds triggered by supernova explosions (Vader 1986; Matteucci & Tornambé 1987; Arimoto & Yoshii 1987; Carraro et al. 2002; Silk 2002) are required.

Another issue concerning the dSph galaxies is the suggestion of a connection between these gas-poor galaxies and late-type gas-rich galaxies (Blue Compact Galaxies - BCGs) in an unified evolutionary scenario, in the sense that one type (BCGs) could evolve into the other (dSph) by means of the consumption of the gas into stars by SF or removal of gas by ram pressure stripping (Lin & Faber 1983; Dekel & Silk 1986; Davies & Phillipps 1988; van den Bergh 1994; Papaderos et al. 1996a).

The BCGs (also called HII Galaxies) are small galaxies with high central surface brightness, large content of neutral gas (up to ~ 10 times the stellar content), low metallicities (from $0.5 Z_{\odot}$ to $0.02 Z_{\odot}$), and ongoing star formation. All these properties lead to the idea that the BCGs should be poorly evolved objects either young or which have undergone few episodes of star formation separated by long quiescent periods. The last hypothesis seems to be the most likely for the majority of the BCGs (see Kunth & Östlin 2000 for a review).

A great deal of theoretical models for BCGs were proposed in order to explain the observed abundances (Matteucci & Chiosi 1983; Matteucci & Tosi 1985; Pilyugin 1993; Carigi et al. 1994; Marconi, Matteucci & Tosi 1994; Kunth, Matteucci & Marconi 1995). They all derived similar scenarios for the chemical evolution in these systems: the IMF is in general the same everywhere with a slope similar to the Salpeter (1955) one, galactic winds with varying efficiencies are necessary to explain the observational data, and the star formation is discontinuous and characterized by short bursts separated by quiescent periods. The same scenario was adopted by Bradamante, Matteucci & D'Ercole (1998 - hereafter BMD) who proposed a model with short and intense bursts of activity where the stellar energetics and the presence of dark matter were taken properly into account in order to explain the observed N/O, C/O and O/Fe ratios. Their model suggested that the number of bursts should be between 1 and 10 with an efficiency of star formation varying from 0.1 to 7 Gyr^{-1} and a Salpeter IMF. They also concluded that the BCGs should be dominated by dark matter, with a ratio between dark and luminous matter $R = 1-50$ in order to be gravitationally bound against the intense starbursts, and that galactic winds are differential, in the sense that is likely that some chemical elements are preferentially lost from the system.

More recently, Recchi et al. (2001, 2002), analysed the effects of starbursts on the dynamical and chemical evolution of BCGs, by taking into account, in detail, the chemical and energetical contributions from type II (SNe II) and type Ia (SNe Ia) supernovae. The dynamical and chemical evolution of the ISM was followed by means of a two-dimensional hydrodynamical code coupled with chemical yields originating from SNe II, SNe Ia and single intermediate mass stars (IMS). They concluded that a galactic wind develops as a consequence of the starburst and carries out of the galaxy mostly the metal-enriched gas and that the wind indeed is differential, in the sense that the elements produced by type Ia SNe are lost slightly more efficiently than others. The

reason for this resides in the fact that when this kind of explosions (SNe Ia) occurs, the medium is hotter and more rarefied than when the SNe II occurs. In such a case, the efficiencies of energy transfer of supernovae type II and type Ia, contrary to BMD, are not the same. As the SNe Ia explosions occur in hotter a more rarefied medium, their energy is more efficiently thermalized into the ISM and, consequently, their efficiency of energy transfer is higher.

In this paper, in order to understand the chemical evolution histories of dSph galaxies and explore the possible connection between these galaxies and BCGs we use chemical evolution models which treat in details the energetics and take into account the yields of supernovae of type II and Ia as well as IMS. The goal is to follow in detail the evolution of the abundance of several elements in both types of galaxies. The models are based on the work of BMD and follow the recent results for the energetics and winds given in Recchi et al. (2001). These prescriptions are very important since we assume that winds are the main responsible for the low gas content of the dSph galaxies together with the consumption of gas by star formation. The models for dSph galaxies and BCGs differ in the prescriptions for star formation, in the luminous masses, in the wind efficiency and in the star formation efficiency.

The comparison of the models for both the dSph galaxies and BCGs with the observational data of Damped Lyman α Systems (DLAs) could also help to understand the nature of these systems, since recent works using chemical and chemodynamical evolution models suggested that the progenitors of DLAs could be irregular galaxies such as the Large Magellanic cloud and/or BCGs (Calura, Matteucci & Vladilo 2003) and dwarf ellipticals (Lanfranchi & Friaça 2003), respectively.

The paper is organized as follows: in Sect. 2 we present the observational data concerning the dSph galaxies and BCGs, in Sect. 3 the adopted chemical evolution models and star formation prescriptions are described, in Sect. 4 we describe the results of our models, which are compared to observational data from DLAs in Sect. 5 and finally in Sect. 6 we draw some conclusions. We use the solar abundances measured by Grevesse & Sauval (1998) when the chemical abundances are normalized to the solar values ($[X/H] = \log(X/H) - \log(X/H)_{\odot}$) and a $H_0 = 70 \text{ km sec}^{-1} \text{ Mpc}^{-1}$, $\Omega_m = 0.3$, $\Omega_{\Lambda} = 0.7$ cosmology is assumed throughout the paper.

2 DATA SAMPLE

The data sample collected for dSph galaxies consists of abundances of iron and some α -elements such as O, Mg, Si and Ca obtained from the most recent high-resolution spectroscopy of red giant stars in 8 dSph galaxies of the Local Group (Smecker-Hane & McWilliam 1999; Bonifacio et al. 2000; Shetrone, Coté & Sargent 2001; Shetrone et al. 2003). As the abundances were measured in stars within a range of ages it is possible to study the evolution with time of each galaxy or the dSph galaxies as a whole, if one assumes that these galaxies have a similar chemical evolution history. This is, though, a point of controversy, since there are suggestions in the literature that the local dSph galaxies exhibit complex star formation histories (Smecker-Hane & McWilliam 1999;

Hernandez, Gilmore & Valls-Gabaud 2000). We will show that all these galaxies chemically evolve in a similar way, in spite of their different star formation histories, which are used as a constraint for the number, epoch and duration of the bursts of SF in the models. Besides the abundance ratios, we compare the predictions of the chemical evolution models to other properties of the dSph galaxies taken from the review of Mateo (1998).

For BCGs, the collected abundances of the elements N, O, C, Si and Fe were determined from measurements in HII regions from either ground-based high resolution spectroscopy or from UV observations of the Hubble Space Telescope (Garnett et al. 1995; Kobulnicky & Skillman 1996; Izotov & Thuan 1999). The diagram of the abundance ratios versus oxygen (e.g. N/O versus O/H) should not be viewed, in this case, as an evolutionary diagram because each point represents a different galaxy as it is seen at the present time, giving no clear information about their evolution (see Chiappini, Romano & Matteucci 2003). To compare properly these abundances with the prediction of the models one should only look at their final points, i.e the predicted present day abundances. However, as these galaxies might have been formed at different epochs, we plot also the evolutionary lines in order to take into account possible different ages. It should be mentioned, though, that each point is a galaxy that could have followed a particular evolutionary track.

3 MODELS

In order to study the chemical evolution and star formation histories of dSph galaxies and BCGs we use an updated version of the model of BMD in two different scenarios. The first one, representing the dSph galaxies, is characterized by a single and long star formation episode whereas several short episodes of star formation separated by long quiescent periods are assumed for the BCGs. These models allow one to follow in detail the evolution of the abundances of several elements, starting from the matter reprocessed by the stars and restored into the ISM by winds and type II and Ia supernova explosions.

The main features of the models are the following:

- one zone with instantaneous and complete mixing of gas inside this zone;
- no instantaneous recycling approximation, i.e. the stellar lifetimes are taken into account;
- the evolution of several chemical elements (H, D, He, C, N, O, Mg, Si, S, Ca and Fe) is followed in detail;
- the efficiencies of energy transfer adopted are $\eta_{SNeII} = 0.03$, $\eta_{SNeIa} = 1.0$ and $\eta_w = 0.03$ for SNe II, SNe Ia and stellar winds, respectively (see BMD for more details);
- the nucleosynthesis prescriptions include the yields of: Thielemann, Nomoto & Hashimoto (1996) for massive stars ($M > 10M_{\odot}$), van den Hoeck & Groenewegen (1997) for low and intermediate mass stars ($0.8 \leq M/M_{\odot} \leq 8$) and Nomoto et al. (1997) for type I a SNe.

In our scenario, the dSph galaxies form as a result of a continuous infall of pristine gas until a mass of $\sim 10^8 M_{\odot}$ is accumulated. One crucial feature in the evolution of

these galaxies is the occurrence of galactic winds, which develop when the thermal energy of the gas equals its binding energy (Matteucci & Tornambé 1987). This quantity is strongly influenced by assumptions concerning the presence and distribution of dark matter (Matteucci 1992). A diffuse ($R_e/R_d=0.1$, where R_e is the effective radius of the galaxy and R_d is the radius of the dark matter core) but massive ($M_{dark}/M_{Lum} = 10$) dark halo has been assumed for both models. The BCGs are built almost in the same way, but the total masses eventually reached are higher ($\sim 10^9 M_\odot$) as suggested by observations (these galaxies show large HI halos - Mateo 1998). The occurrence of galactic winds in BCGs is not as important as for dSph galaxies. Actually, for some star formation efficiencies, winds in these systems do not even develop.

3.1 Theoretical prescriptions

The time-evolution of the fractional mass of the element i in the gas within a galaxy, G_i , is described by the basic equation:

$$\dot{G}_i = -\psi(t)X_i(t) + R_i(t) + (\dot{G}_i)_{inf} - (\dot{G}_i)_{out} \quad (1)$$

where $G_i(t) = M_g(t)X_i(t)/M_{tot}$ is the gas mass in the form of an element i normalized to a total fixed mass M_{tot} and $G(t) = M_g(t)/M_{tot}$ is the total fractional mass of gas present in the galaxy at the time t . The quantity $X_i(t) = G_i(t)/G(t)$ represents the abundance by mass of an element i , with the summation over all elements in the gas mixture being equal to unity. $\psi(t)$ is the fractional amount of gas turning into stars per unit time, namely the SFR. $R_i(t)$ represents the returned fraction of matter in the form of an element i that the stars eject into the ISM through stellar winds and supernova explosions; this term contains all the prescriptions concerning the stellar yields and the supernova progenitor models. The two terms $(\dot{G}_i)_{inf}$ and $(\dot{G}_i)_{out}$ account for the infall of external gas and for galactic winds, respectively. The prescription adopted for the star formation history is the main feature which characterizes a particular morphological galactic type.

The SFR $\psi(t)$ has a simple form and is given by:

$$\psi(t) = \nu G(t) \quad (2)$$

The quantity ν is the efficiency of star formation, namely the inverse of the typical time-scale for star formation, and is expressed in Gyr^{-1} .

In both cases, dSph galaxies and BCGs, ν is varied, but in a larger range for dSph galaxies and with lower values than the ones assumed for BCGs. The star formation proceeds even after the onset of the galactic wind but at a lower rate since a large fraction of the gas ($\sim 10\%$) is carried out of the galaxy. In dSph galaxies the star formation is characterized by 1 or 2 long episodes of star formation (3-13 Gyr), according to the star formation history of each individual galaxy as inferred by CMDs taken from Dolphin (2002) and Hernandez, Gilmore & Valls-Gabaud (2000). We also computed a model (the standard model) for the whole sample of dSph galaxies using one long burst of star formation starting at a galactic age of 1 Gyr with a duration of 8 Gyr. For BCGs, on the other hand, we adopted a SF proceeding in short bursts separated by long quiescent periods. The num-

Table 1. Model parameters for dSph galaxies and BCGs. M_{tot} is the baryonic mass of the galaxy, ν is the star-formation efficiency and w_i is the wind efficiency.

	$M_{tot}(M_\odot)$	$\nu(\text{Gyr}^{-1})$	w_i	IMF
dSph	$5 * 10^8$	0.01-1	10	Salpeter
BCGs	$6 * 10^9$	0.1-0.9	0.5	Salpeter

ber of the bursts varies from 2 to 7 and the duration of each burst from 10 to 200 Myr.

The rate of gas infall is defined as:

$$(\dot{G}_i)_{inf} = Ae^{-t/\tau} \quad (3)$$

with A being a suitable constant and τ the infall timescale which is assumed to be 0.5 Gyr.

The rate of gas loss via galactic winds for each element i is assumed to be proportional to the star formation rate at the time t :

$$\dot{G}_{iw} = w_i \psi(t) \quad (4)$$

where w_i is a free parameter describing the efficiency of the galactic wind. The wind is assumed to be differential, i.e. some elements, in particular the products of SNe Ia, are lost more efficiently than others from the galaxy (Recchi et al. 2001). This fact translates into slightly different values for the w_i corresponding to different elements. Here we will always refer to the maximum value of w_i . The efficiency of the wind is different for each type of galaxy, being much higher for dSph galaxies than for BCGs.

The initial mass function (IMF) is usually assumed to be constant in space and time in all the models and is expressed by the formula:

$$\phi(m) = \phi_0 m^{-(1+x)} \quad (5)$$

where ϕ_0 is a normalization constant. In both cases we assumed a Salpeter-like IMF (1955) ($x = 1.35$), but tested also a flatter IMF ($x = 1.1$) and the Scalo (1986) prescription ($x = 1.35$ for $0.1 \leq m/m_\odot \leq 2$, $x = 1.7$ for $2 < m/m_\odot \leq 100$), always in the mass range $0.1 - 100 M_\odot$.

In table 1 we summarize the adopted parameters for the models of BCGs and dSph galaxies.

4 RESULTS

4.1 Dwarf Spheroidal Galaxies

In order to understand the chemical evolution and star formation histories of the dSph galaxies of the Local Group, we compare the predictions of the chemical evolution model described in the previous section with the observed [O/Fe], [Si/Fe], [Ca/Fe] and [Mg/Fe] ratios. The final gas content and total mass of the modelled galaxy are also compared to the observational data.

Different models are computed by varying some parameters such as the star formation efficiency, the number of the bursts, the duration of each burst, the wind efficiency,

Table 2. Models for dSph galaxies. n , t and d are the number, time of occurrence and duration of the bursts, respectively, and ν the range of SF efficiencies.

model	n	t(Gyr)	d(Gyr)	ν (Gyr^{-1})
standard model	1	1	8	0.01-1
Sextan	1	1	8	0.01-0.4
Sculptor	1	0	7	0.03-0.5
Sagittarius	1	0	13	0.5-3.0
Draco	1	6	4	0.005-0.05
Ursa Minor	1	0.5	3	0.05-0.5
Carina	2	6/10	3/3	0.01-0.5

the total mass of the galaxy and the IMF prescription. The first choices for the number and duration of the bursts were taken from the star formation histories inferred by CMDs of a sample of Local Group dSph galaxies and the star formation efficiency was fixed at low values as suggested by the observed abundance ratios (see Table 2). The other parameters were tuned in order to match the observed quantities.

We started the study by considering the data sample as a whole, without separating individual galaxies. The similarity of the abundance patterns of the elements studied here for all the galaxies of the sample justifies this procedure and suggests that there is an uniformity in the chemical evolution of these galaxies, in spite of their different star formation histories (Tolstoy et al. 2003).

One or two bursts with long duration (3 to 8 Gyr), a low efficiency for the star formation ($\nu < 1 Gyr^{-1}$) and a high wind efficiency ($w_i > 5$) were chosen as initial parameters in order to reproduce the observed abundance ratios. We found that the most important parameter to reproduce the observed ratios is the star formation efficiency and the one which best regulates the gas content, at a given SFR, is the wind efficiency. Three series of models with different choices for the IMF were computed: one with a Salpeter-like IMF (1955), one with Scalo (1986) and a last one with an exponent $x=1.1$. The models with a Scalo IMF fail in reproducing the observed abundance ratios, since they generally produce too low $[\alpha/Fe]$ ratios for a given SF efficiency, thus were discarded. The other two models, with Salpeter and a flatter IMF, require both a star formation efficiency in the range $\nu \sim 0.01 - 1 Gyr^{-1}$ and a wind efficiency between $w_i \sim 5 - 15$ for a SF proceeding in one long episode of activity. The model with a flatter IMF, however, predicted too large $[\alpha/Fe]$ abundance ratios and HI mass/total mass ratios so we adopted the Salpeter IMF. Figure 1 shows the observed abundance ratios compared with the predictions of the models with different efficiencies of star formation, which are characterized by one single episode of activity starting at 1 Gyr and lasting for 8 Gyr. The wind efficiency is $w_i = 10$ and a Salpeter IMF is adopted (from now on the standard model). The different symbols in Figure 1 represent stars in different galaxies and the various lines correspond to different SF efficiencies.

We noticed an interesting feature in the predicted abundance ratios: an abrupt decrease of $[O/Fe]$ and $[Mg/Fe]$ and a smoother one for $[Si/Fe]$ and $[Ca/Fe]$ starting at $[Fe/H] \geq -2.0$ for the model with $\nu = 0.01 Gyr^{-1}$ and at $[Fe/H] \geq -1.0$ for the one with $\nu = 1 Gyr^{-1}$. These are the metal-

licities reached by the ISM when the wind develops. The behaviour shown in Figure 1 has several reasons. The most important one is that after the onset of the wind the star formation gradually vanishes and this decreases the $[\alpha/Fe]$ ratios since the α -elements are no more produced whereas Fe is produced by type Ia SNe. In addition, we should consider the effect of the galactic wind: as the efficiency of the wind is high and the wind is differential, a large amount of the processed gas is lost from the galaxy in different fractions for different elements (D’Ercole & Brighenti 1999; McLow & Ferrara 1999). When the SNe Ia explode the products of these explosions find an ISM hotter and more rarefied due to the effect of the previous explosions of SNII and are able to leave the galaxy more efficiently than the products of type II supernovae (Recchi et al. 2001). As a consequence, the wind is more enriched in iron-peak elements, the principal products of SNe Ia, than in α elements which are produced mainly in massive stars and injected into the ISM by SNII explosions (Woosley & Weaver 1995; Thielemann, Nomoto & Hashimoto 1996). However, this effect is small in our formulation and it acts more on the absolute Fe abundance and on the models with lower star formation efficiency (see for example the inversion of the $[Fe/H]$ in the model corresponding to $\nu = 0.01 Gyr^{-1}$). The decrease in the $[\alpha/Fe]$ ratios is lower for Si and Ca than for O and Mg and the reason resides in the fact that Si and Ca are produced in type Ia SNe more than O and Mg.

The behaviour of the $[\alpha/Fe]$ ratios is consistent with the observed values which show a clear decrease at metallicities higher than $[Fe/H] \sim -1.8$ for $[O/Fe]$ and $[Mg/Fe]$ and a less intense decrease for $[Si/Fe]$ and $[Ca/Fe]$ at the same metallicity. There are some points, however, which lie above the predictions of the models. Almost all of them are stars from the Sagittarius dSph galaxy. This suggests only that this galaxy requires a higher star formation efficiency than the values used in the standard model (see Figure 2). From Figure 1 one can see also that the wind is not important only in regulating the remaining gas content, but also in determining the pattern of abundance ratios, since the abundance ratios observed in many of the stars of the local dSph galaxies are reproduced only with the occurrence of an intense wind. In particular, the effect of the wind is to decrease the absolute Fe abundance while the $[\alpha/Fe]$ ratios are not so affected since both α -elements and Fe are lost. The fact that Fe is lost with a slightly higher efficiency than the α -elements is not the dominant factor in these plots. We have run also models with a normal galactic wind (same efficiency for all the elements) and the difference in the resulting curves is quite small but the effect is more evident in the model with the lowest star formation efficiency. The range adopted for the star formation efficiency allows the standard model to reproduce the data of all the studied galaxies, assuming that they have similar star formation histories, in particular one long starburst. The differences in the abundance ratios in different galaxies are then mainly a combined effect of the wind and star formation efficiencies rather than due to the detailed star formation histories. In order to check this assumption we computed different models for each galaxy using the star formation histories inferred by CMDs (Hernandez, Gilmore & Valls-Gabaud 2000; Dolphin 2002) as a constraint on the number, epoch and duration of the bursts (see Table 2). The efficiency of the star formation was varied

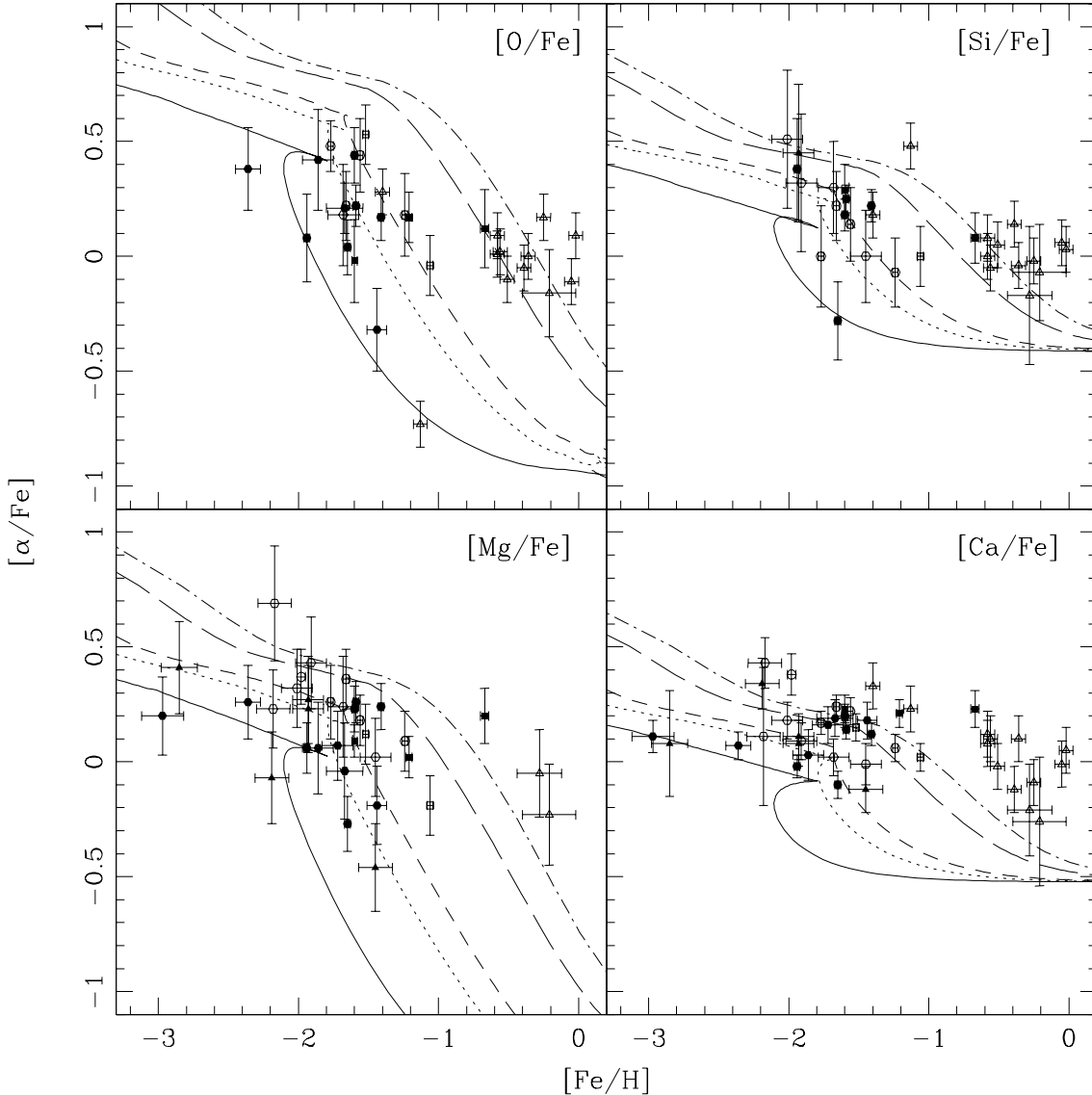


Figure 1. $[\alpha/\text{Fe}]$ vs. $[\text{Fe}/\text{H}]$ observed in dSph galaxies compared to the predictions of the standard model for dSph galaxies. The different lines correspond to different SF efficiencies (in Gyr^{-1}): 0.01 (solid line), 0.05 (dotted), 0.1 (dashed), 0.5 (long-dashed), 1.0 (dotted-dashed). The signs represent stars of different galaxies: Sagittarius (open triangles), Draco (filled hexagons), Carina (filled circles), Ursa Minor (open hexagons), Sculptor (open circles), Sextan (filled triangles), Leo I (open squares) and Fornax (filled squares). The occurrence of the wind is marked by the change in the slope of the curves.

to get the best agreement with all the α/Fe ratios observed in each galaxy. The other parameters as the efficiency of the wind, IMF, initial mass, amount and distribution of dark matter, were the same as in the standard model. We used the 6 galaxies for which there are enough data to compare with the predictions of the models, in particular Draco, Ursa Minor, Sculptor, Sagittarius and Carina, for which a star formation history has been inferred (see table 2 for more details). For the last one, Sextan, we used the prescriptions of the standard model. In Figure 2 we show the predictions of the individual models with different SF efficiencies compared with the $[\text{Si}/\text{Fe}]$ (or $[\text{Mg}/\text{Fe}]$ when Si is not available) observed in each galaxy. It should be mentioned that the SF efficiencies determined for each galaxy were inferred from the comparison with the four abundance ratios observed,

even though only the data for one ratio are shown in Figure 2.

When using the number, duration and epoch of the bursts given by the inferred star formation histories, coupled with the star formation efficiencies given by the standard model, the data of all galaxies are well reproduced. This suggests that, indeed, the most important parameter to explain the observed distributions is the efficiency of the star formation. One can see, from Figure 2, that 4 (Carina, Sextan, Sculptor and Ursa Minor) out of the 6 galaxies require a similar range of SF efficiencies, $\nu = 0.01\text{--}0.5 Gyr^{-1}$. The other 2 galaxies are reproduced by either a lower (Draco) or a higher ν (Sagittarius).

The differences in the chemical evolution among these galaxies can be clearly seen in Figure 3, where the predicted Fe-age relations are plotted for each individual dSph galaxy.

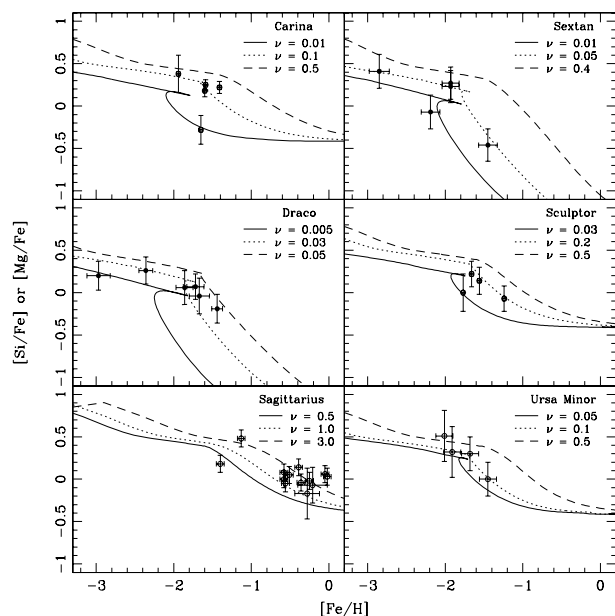


Figure 2. Predictions of the models for individual dSph galaxies compared to observed $[\text{Si}/\text{Fe}]$ (open circles) or $[\text{Mg}/\text{Fe}]$ (filled circles). The lines represent different SF efficiencies.

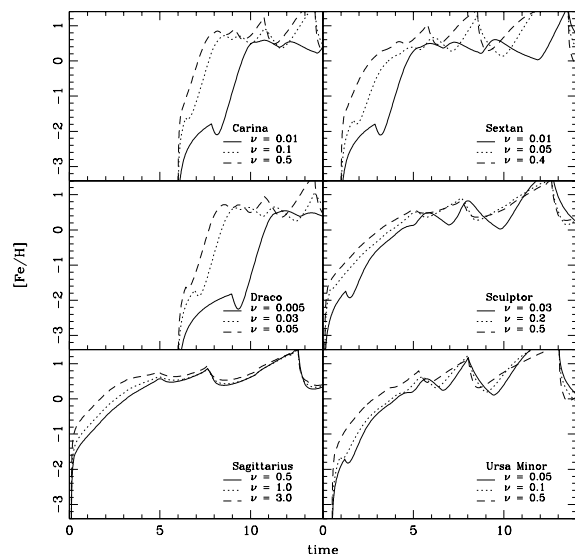


Figure 3. $[\text{Fe}/\text{H}]$ as a function of time as predicted by the models for each individual dSph galaxy. The different lines represent different SF efficiencies.

At variance with the abundance ratios, $[\text{Fe}/\text{H}]$ is more sensitive to the details of the SF history of the galaxy as one can see in Figure 3. The galaxies could be divided in two groups: one including four galaxies (Sagittarius, Ursa minor, Sculptor and Sextan), where the SF starts at early times, and another one with the remaining two galaxies (Draco and Carina), where the SF starts at an older cosmic time. In the galaxies of the second group the $[\text{Fe}/\text{H}]$ reach the solar value faster ($\sim 1 - 2$ Gyr after the onset of the SF) than in the galaxies of the first group ($\sim 2 - 5$ Gyr)

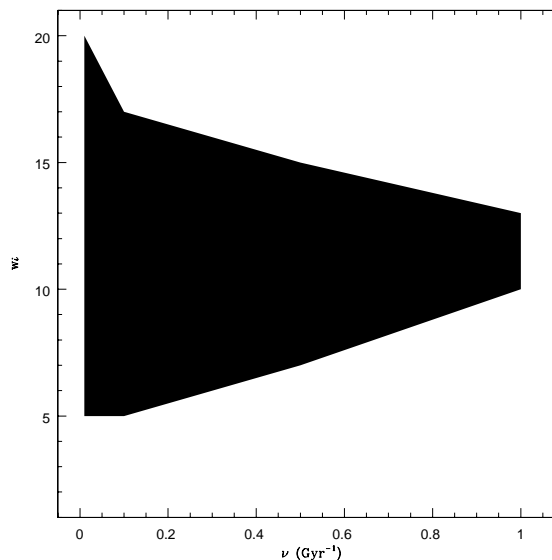


Figure 4. Values of the wind efficiency which fit the data of the dSph galaxies as a function of the SF efficiency. The shaded area correspond to the values of both parameters which reproduce the observed data.

and there is a narrower range of ages for the stars which are younger (Draco and Carina) if compared to the other galaxies at the same metallicity. Consequently, we predict that one should observe a wide spread in ages of the stars of Sagittarius, Sculptor, Ursa Minor and Sextan (a little bit lower in this latter) whereas the observed stars of Carina and Draco should have ages within a short interval of some Gyrs. It should be mentioned, though, that this last statement depends on the adopted SF histories. Another point that should be viewed with care is the Fe abundances which reach high values, well above the ones observed in stars of the dSph galaxies of the local group. The predicted $[\text{Fe}/\text{H}]$ is, in fact, the abundance expected in the ISM, and as the SF gradually vanishes and the galactic wind develops, the number of stars formed after this stage is very low. This stage corresponds to a metallicity range of $[\text{Fe}/\text{H}] \sim -1.5 - -0.5$ dex, depending on the SF efficiency, and the number of stars formed with metallicities higher than these will decrease as the metallicity in the ISM increases.

The adopted wind efficiency is the same for all galaxies, even though differences in the rate of wind might exist. These differences in the wind rate between galaxies are accounted for by the various SF efficiencies, since the rate of the wind is assumed to be proportional to the SFR. As the SF efficiencies are similar for the galaxies of the studied sample, but not equal, so it is the wind rate. The wind efficiency establishes how intense is the wind, i.e. the amount of material which is actually lost from the galaxy. The results of our model for the present day total mass and gas content of the galaxies show that the range of wind efficiencies adopted here provides a good fit to the observed data (see Table 3), but it can vary depending on the adopted SF efficiency (Figure 4). If the wind efficiency is lowered below $w_i = 5$, the final gas mass in the modelled galaxies with high SF efficiencies ($\nu \geq 0.1 \text{ Gyr}^{-1}$) would be much higher than

Table 3. Predictions of the models for dSph galaxies compared to observations. M_{tot} is the present day total mass of the galaxy, M_{HI}/M_{tot} is the present day ratio between the HI mass and total mass.

	M_{tot} ($10^6 M_{\odot}$)		M_{HI}/M_{tot}		1 ^o burst (Gyr)		2 ^o burst (Gyr)	
	obs	mod	obs	mod	obs	mod	obs	mod
standard model	6.4-68 ^d	6.4-85.2	<0.004 ^d	0.0001-0.0004	-	1-9	-	-
Sextan	19 ^a	6.4-46.4	<0.001 ^a	0.0001-0.0004	-	1-9	-	-
Sculptor	6.4 ^a	9.6-40.1	0.004 ^a	0.0002-0.0003	0-7 ^c	0-7	-	-
Sagittarius	-	40.1-150.7	<0.001 ^a	0.0002	0-13 ^c	0-13	-	-
Draco	22 ^a	5-21.1	<0.001 ^a	0.0002-0.0007	6-10 ^b	6-10	-	-
Ursa Minor	23 ^a	12.5-47.6	<0.002 ^a	0.0002-0.0004	0-3 ^b	0.5-3.5	-	-
Carina	13 ^a	6.6-56.5	<0.001 ^a	0.0004-0.0006	6-9 ^b	6-9	10-13 ^b	10-13

a - Mateo (1998)

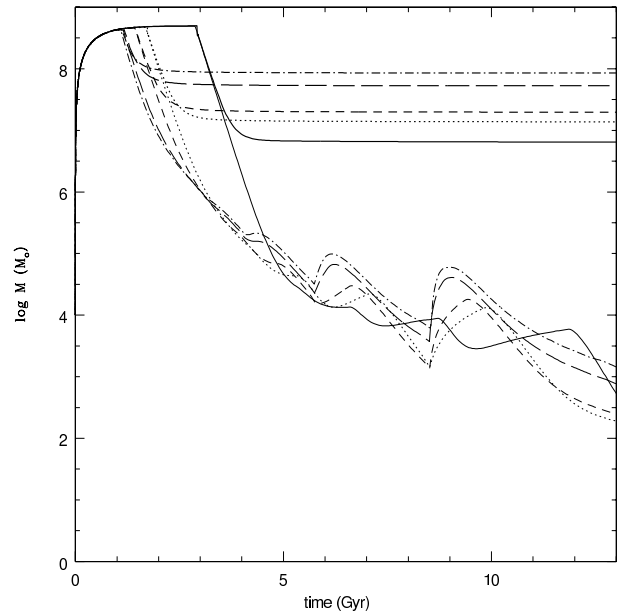
b - Hernandez, Gilmore & Valls-Gabaud (2000)

c - Dolphin (2002)

d - for the whole sample of dSph galaxies in Mateo (1998)

the values observed and the decrease in the abundance ratios of the models with low SF efficiencies ($\nu \leq 0.1 \text{ Gyr}^{-1}$) would not be enough to reproduce the lowest values observed. If, on the other side, w_i were too high ($w_i \geq 20$) the galaxy, in the models with the lowest SF efficiencies ($\nu \leq 0.1 \text{ Gyr}^{-1}$), would loose all the gas content as soon as the wind starts, the star formation would cease and there would not be stars forming with metallicities higher than that in the gas when the wind develops ($[\text{Fe}/\text{H}] \sim -2.0$ for the model with $\nu = 0.01 \text{ Gyr}^{-1}$ and $[\text{Fe}/\text{H}] \sim -1.0$ for the model with $\nu = 1 \text{ Gyr}^{-1}$). On the other hand, in the models with high SF efficiencies a high wind efficiency ($w_i \geq 13$) predicts abundance ratios which would not reproduce the highest values observed. Given these facts and Figure 4, one can conclude that the range of the wind efficiency becomes narrower as the SF efficiencies increases and that a value between $w_i \sim 10 - 13$ can reproduce the observed final masses and abundance ratios independently from the adopted SF efficiency.

In Figure 5 we plot the evolution with time of the total mass (thick lines) of the galaxy and its gas content (thin lines) for the standard model with different efficiencies of star formation (the different lines). The time of the occurrence of the wind varies with the rate of star formation since it depends on the amount of energy which is injected into the ISM. For the model where the star formation is less efficient (solid line), a wind is developed only almost 2 Gyr after the onset of the star formation, but for the cases where the star formation is more intense the wind occurs sooner ($\sim 100 \text{ Myr}$) after the star formation begins. As the wind is very efficient, the gas content and total mass of the galaxy decrease fast in few Gyrs, but after that, the total mass remains almost constant and the amount of gas continues to decrease at a much lower rate, in agreement with Ferrara & Tolstoy (2000). The oscillation in the gas content is due to the duration of the wind and to the contemporary injection of gas into the ISM from dying stars. The results for the total final mass and gas content of the standard model applied to each individual galaxy and compared to observational data are shown in Table 3. It is also shown the number and epochs of the bursts of star formation. The models for each galaxy as well as the standard model are in good agreement with the observational data. The variations of the masses in the models are due to the range of star formation efficiencies

**Figure 5.** Evolution with time of the total mass (thick lines) and gas content (thin lines) as predicted by the standard model for dSph galaxies with different SF efficiencies. The different lines correspond to different SF efficiencies (in Gyr^{-1}): 0.01 (solid line), 0.05 (dotted), 0.1 (dashed), 0.5 (long-dashed), 1.0 (dotted-dashed).

adopted in each model. In general, the larger the star formation efficiency, the higher the total final mass and the lower the final gas mass/total mass ratio, since more stars are formed and consequently more gas is consumed (see also Figure 5).

4.2 Blue Compact Galaxies

The possible scenarios for BCGs proposed in the literature in order to explain the pattern of several abundance ratios consider these galaxies either as young objects, especially those with $12 + \log(\text{O}/\text{H}) \leq 7.6$ (Izotov & Thuan 1999), where primary N produced in massive stars is required to explain the low values of N/O, or older systems which suffered several episodes of star formation separated by long

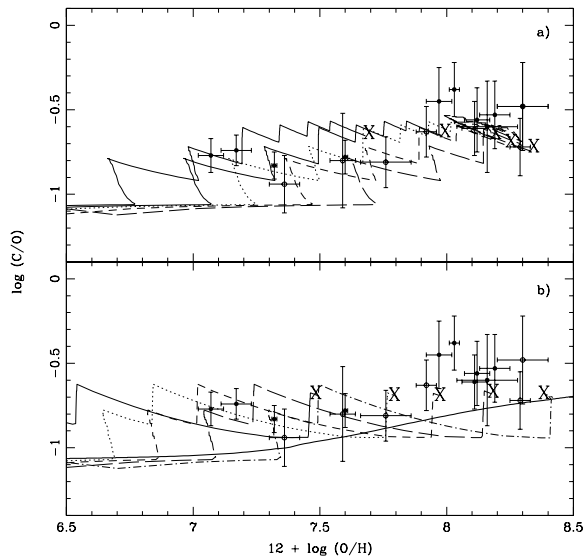


Figure 6. $\log(C/O)$ vs. $12 + \log(O/H)$ observed in BCGs compared to the predictions of the standard model for BCGs with 7 and 4 bursts (panels *a* and *b*, respectively). The lines represent different SF efficiencies (in Gyr^{-1}): 0.1 (solid line), 0.2 (dotted), 0.3 (dashed), 0.5 (long dashed) and 0.9 (dotted-dashed). The solid thick line represents a model with continuous star formation and a SF efficiency $\nu = 0.1 Gyr^{-1}$. The crosses represent the final abundances of the models. Filled symbols are the data from Izotov & Thuan (1999) and open symbols from Garnett et al. (1995).

quiescent periods, in which the low values of N/O are a consequence of the time-delay between the productions of O in massive stars and N in IMS (Marconi, Matteucci & Tosi 1994; Garnett et al. 1997; BMD; Larsen, Sommer-Larsen & Pagel 2001). In order to explore these two possibilities we made use of different galaxy models following the prescriptions and results of BMD and Recchi et al. (2001, 2002), as discussed previously. Other parameters such as the number and duration of the bursts, the efficiency of the star formation and the galactic wind, the slope of the IMF, the production of N, regarding its primary or secondary origin in massive stars, were varied in order to understand the observed distribution of N/O, C/O, Si/O and [O/Fe] versus O/H in BCGs.

First we defined a standard model fixing some parameters: a Salpeter IMF, a star formation efficiency between $\nu = 0.05 - 2 Gyr^{-1}$, a wind efficiency $w_i = 0.5$, a ratio of dark to luminous matter of 10 and only secondary production of N in massive stars. The number and duration of the bursts were then varied in order to get the best fit to the observed distributions. We computed models with 2 bursts and durations between 10 Myr to 1 Gyr and increased the number of bursts up to 7, with duration no longer than 0.2 Gyr each. As the number of the bursts increases, the duration of each burst decreases, otherwise the galaxy is disrupted by galactic winds.

After defining a range for the number of the bursts and their duration we varied also other parameters such as the exponent of the IMF, the star formation and wind efficiencies, and the origin of N in massive stars (primary and/or

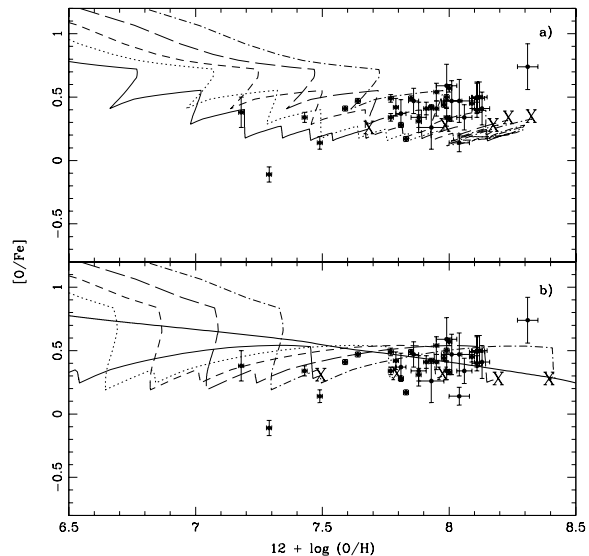


Figure 7. $[O/Fe]$ vs. $12 + \log(O/H)$ observed in BCGs compared to the predictions of the standard model for BCGs with 7 and 4 bursts (panels *a* and *b*, respectively). The solid thick line represents a model with continuous star formation and a SF efficiency $\nu = 0.1 Gyr^{-1}$. The symbols are the same as in Figure 6. The data are from Izotov & Thuan (1999).

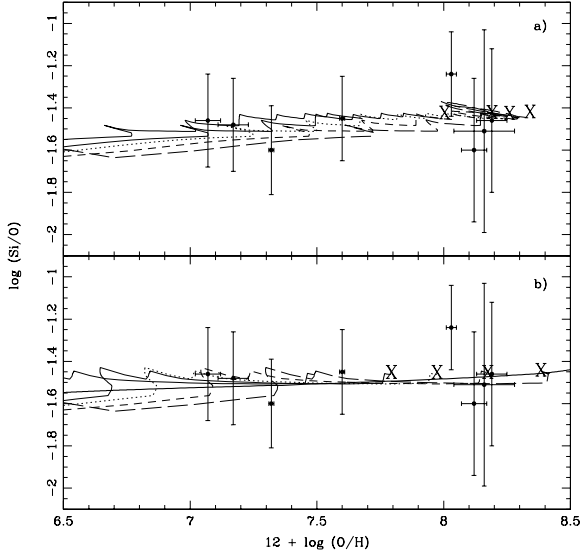
secondary). As already noticed by BMD, the most important parameter to reproduce the observed N/O, C/O, Si/O and [O/Fe] versus O/H distributions is the star formation efficiency. We found that a star formation efficiency in the range $\nu = 0.1-0.9 Gyr^{-1}$ is needed in order to reproduce the majority of the observational constraints when a Salpeter IMF is adopted. The range of values for ν changes when a Scalo IMF is used but remains the same if an exponent $x=1.1$ is adopted. In the case of a Scalo IMF, the values of the star formation efficiency required to reproduce the observed metallicities must be higher but the agreement with the observed abundance ratios is poorer. An IMF with an exponent $x=1.1$ should also be discarded. In this case, in fact, the number of massive stars produced is higher and so the abundance of α elements, the main product of these stars. Consequently, the N/O ratio is well reproduced, especially the lower values, but at the same time, the predicted [O/Fe] ratios become too high and the C/O ratios too low if compared with the observations.

In the range of the star formation efficiency defined above for a Salpeter IMF, models with 2 to 7 bursts are able to reproduce the observed abundance ratio diagrams if proper values for the wind efficiency and durations of the bursts are adopted. The difference between these models is that as the number of bursts increases, increases also the variation in the predicted ratios (sawtooth behaviour) and the spread of the data is better reproduced by the models with 7 bursts (standard model *a* in table 4) in the case of C/O, [O/Fe] and Si/O (panel *a* in Figures 6, 7 and 8, respectively). The N/O, especially the lowest values, are however difficult to be achieved with 7 bursts (panel *a* in Figure 9), without breaking the agreement with the other ratios.

A model with 4 bursts (standard model *b* in table 4),

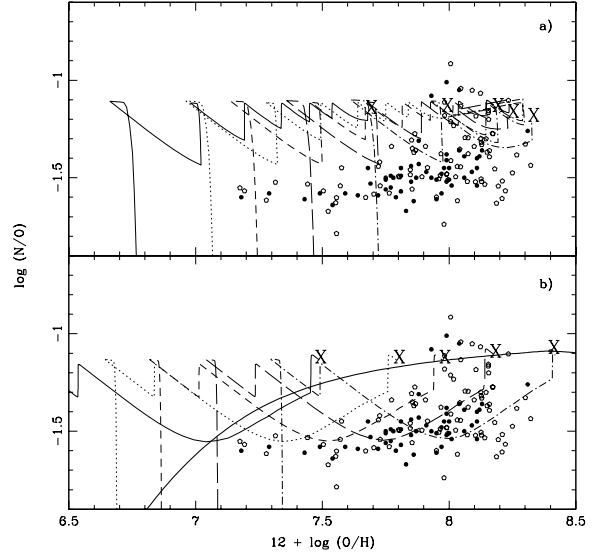
Table 4. Models for BCGs. n , t and d are the number, time and duration of the bursts, respectively, and ν the range of SF efficiencies.

model	n	$t(Gyr)$	$d(Gyr)$	$\nu (Gyr^{-1})$
standard model a	7	0.5/1/2/5/7/11/13.9	0.05/0.05/0.05/0.05/0.05/0.05/0.1	0.1-0.9
standard model b	4	1/10/13/13.98	0.02/0.01/0.2/0.02	0.1-0.9

**Figure 8.** $\log(Si/O)$ vs. $12 + \log(O/H)$ observed in BCGs compared to the predictions of the standard model for BCGs with 7 and 4 bursts (panels *a* and *b*, respectively). The solid thick line represents a model with continuous star formation and a SF efficiency $\nu = 0.1 Gyr^{-1}$. The symbols are the same as in Figure 6. The data are from Izotov & Thuan (1999).

instead, reproduces all the values of N/O, including the low ones, and fits the other ratios as well (panel *b* in Figures 6, 7, 8 and 9) if the epochs and durations of the bursts are properly chosen. A first short burst occurring at 1 Gyr with a duration of 20 Myr and three more recent bursts at 11, 13 and 13.98 Gyr lasting for 10, 200 and 20 Myr, respectively, produce the best fit to the data. The low values of N/O are achieved during the third burst when the value of this ratio decreases due to the production and injection of O in the ISM by massive stars. The low values for N/O at low O/H, in this case, are not characteristic of very young systems as suggested in the literature (Izotov & Thuan 1999) since it is necessary to have at least two previous bursts in order to reproduce these values. Actually, these are old systems with several stellar populations formed in different bursts at different epochs, as suggested by the colours of BCGs indicating an underlying old population (Papaderos et al. 1996b; Doublier et al. 1997, 2000; Marlowe, Meurer & Heckman 1999).

At this point it should be mentioned that the predicted final abundance ratios of all the models (the crosses in the figures) are in agreement with the observed ratios, except for the model with 4 bursts and $\nu = 0.9 Gyr^{-1}$ (dotted-dashed line in panel *b* in Figures 6, 7, 8 and 9). This model,

**Figure 9.** $\log(N/O)$ vs. $12 + \log(O/H)$ observed in BCGs compared to the predictions of the standard model for BCGs with 7 and 4 bursts (panels *a* and *b*, respectively). The solid thick line represents a model with continuous star formation and a SF efficiency $\nu = 0.1 Gyr^{-1}$. The symbols are the same as in Figure 6. Filled symbols are the data from Izotov & Thuan (1999) and open symbols from Kobulnicky & Skillman (1996).

in fact, indicates that systems with higher SFR should be younger in order to fit the data. In particular, the evolutionary lines suggest that: younger systems (no more than 1 Gyr) with the same evolutionary history can also be representative of the population of BCGs. This is especially true for the galaxies with low values of N/O at low O/H, which are reproduced by the models during their third burst of SF which occurred 1 Gyr before the present day burst. The almost constant values of N/O (~ -1.6 dex) of these systems could, therefore, be representative of an isochrone since all of them are reached at a galactic age of 13 Gyr.

We also runned models with continuous star formation (thick solid line in Figures 6, 7, 8 and 9) in the same range of SF efficiencies used in the bursting models ($0.1 - 0.9 Gyr^{-1}$). In this case, the predictions of the models can hardly reproduce at the same time the O/Fe, C/O, Si/O and N/O ratios during the evolution of the galaxy and predict a too high present day O/H (which lies out of the range of the plots) compared to the ones observed in the majority of the BCGs. Besides that, the amount of gas compared to the mass of stars is lower than the ones inferred for this type of galaxy. One can conclude, therefore, that a continuous star forma-

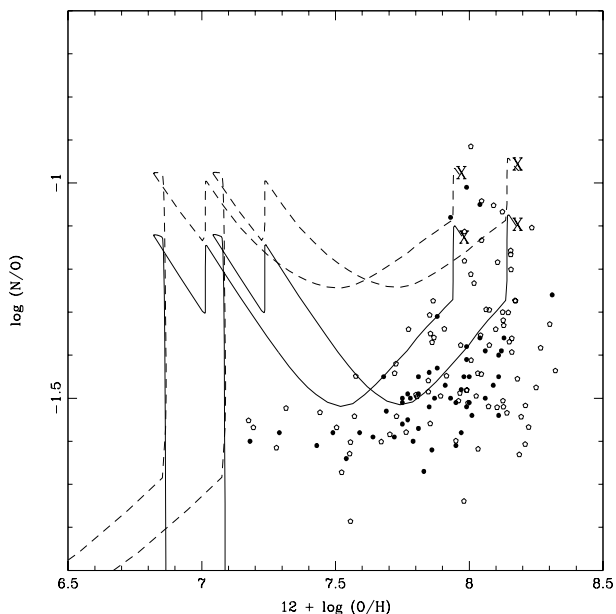


Figure 10. $\log(N/O)$ vs. $12 + \log(O/H)$ observed in BCGs compared to the predictions of the standard model for BCGs with 4 bursts and $\nu = 0.3$ and 0.5 Gyr^{-1} assuming primary production of N in massive stars in different amounts (solid and dashed lines). Filled symbols are the data from Izotov & Thuan (1999) and open symbols from Kobulnicky & Skillman (1996). The crosses represent the final points of the models.

tion may not be a representative scenario for the population of BCGs.

It is worth noticing that the production of primary N in massive stars is not required in order to reproduce the observed N/O, as already noticed by Chiappini, Romano & Matteucci (2003), who studied the origin of carbon, oxygen and nitrogen using chemical evolution models for our Galaxy, more massive disk galaxies and irregular galaxies. In Figure 10 are shown the predictions of the models with 4 bursts when different amounts of primary N produced by massive stars are assumed. The prescriptions for the production of primary nitrogen are the same as in Matteucci (1986). In fact, when large amounts of primary N produced by massive stars are adopted in our models, the predicted N/O ratios are increased and the evolutionary lines grow too fast thus producing a result at variance with the data (dashed lines in Figure 10). Only if very low amounts of N are produced by massive stars, roughly in agreement with the yields predicted by models of stellar evolution including rotation (Meynet & Maeder 2002), this effect would hardly be noticed and the predictions of the models would still reproduce the observed distributions (solid lines in Figure 10).

4.3 Connection between dSphs and BCGs

Dwarf spheroidal galaxies are evolved systems, as witnessed by the lack of detectable ISM. The evolution in these systems could occur in two ways: one type of dwarf galaxy could evolve to another type due to internal (SF, winds) or external (mergers, interactions) effects. Alternatively, the type of the galaxy was determined by the initial conditions and no further change in the morphology has occurred since then.

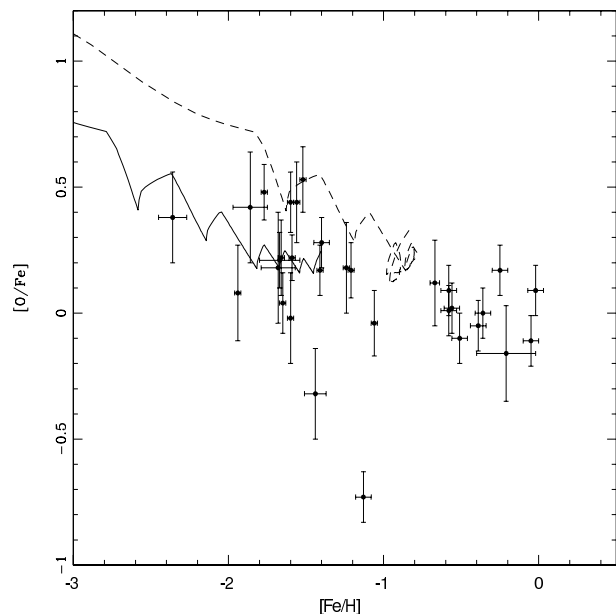


Figure 11. $[O/Fe]$ vs. $[Fe/H]$ observed in dSph galaxies compared to the predictions of the standard model for BCGs with 7 bursts. The solid line represents a model with a SF efficiency $\nu = 0.1 \text{ Gyr}^{-1}$ and the dashed line represents a model with $\nu = 0.9 \text{ Gyr}^{-1}$. No model for dSph galaxies can fit the data for the BCGs.

Here, we focus on the possible connection between different types of dwarf galaxies in an unified evolutionary scenario.

Among the scenarios proposed so far, the one which connects BCGs and dSph galaxies could be investigated through the chemical evolution models described in the previous sections. In this scenario a starburst in a BCG gives rise to a super wind which removes all the gas of the galaxy and halts the SF, giving rise to a dSph galaxy. We see, however, that the chemical evolution histories inferred by the models which give the best match to the observational data of BCGs and local dSph galaxies exhibit marked differences. In particular, the major differences are related just to the SF history and to the galactic wind. While the observed distributions of N/O, C/O, Si/O and $[O/Fe]$ in BCGs are reproduced by models with SF characterized by short and repeated bursts separated by long quiescent periods, the abundance ratios of local dSph galaxies require a SF which proceeds in one (or two) long episodes of activity. The SF efficiencies of the two models also differ even though they overlap in the highest values. The similarity between the SF efficiencies, however, could raise the question whether a bursting SF could reproduce the dSph data or the distribution of abundance ratios in BCGs could be fitted by models characterized by one or two long bursts. The latter possibility is very difficult to achieve, if not improbable (thick solid lines in Figures 6, 7, 8 and 9), but the former is more likely and was already suggested for some dSph galaxies such as Carina. In this case, however, the very low values of α/Fe at high metallicities, especially O and Mg, are not reproduced by this kind of model, as one can see in Figure 11, where we show the observed $[O/Fe]$ ratio in dSph galaxies compared to the predictions of the model applied to BCGs.

The lack of agreement between the models with several

bursts and a low wind efficiency and the data of dSph galaxies clarifies the different roles played by the wind and the SF in the evolution of BCGs and dSph galaxies. As already seen in section 4.1, the occurrence of a wind is a crucial feature not only in the evolution of the total baryonic mass and gas content, but also in the chemical enrichment history of the dSph galaxies: a high wind efficiency ($w_i = 5 - 15$) is required in order to match the observed abundance ratios and stellar masses. On the other hand, the distribution of abundance ratios in BCGs are reproduced by a model with a low wind efficiency, $w_i = 0.5$. Little variations in this value would not change the results as long as $w_i < 1$. If the wind efficiency is larger than $w_i = 1$ the variations in the predicted abundance ratios would be much more intense and would produce a poorer fit to the data. Besides that, the final gas masses of these galaxies would be well below the observed ones. These low values mean that the occurrence of the galactic winds in BCGs does not influence significantly their evolution. In fact, in the models with the lowest SFR, galactic winds do not even develop. Besides that, a model with short episodes of SF separated by long quiescent periods within the range of SF efficiency adopted here is not able to produce the relatively high oxygen abundances observed in dSph galaxies in comparison with the ones observed in BCGs.

From the above remarks, it seems unlikely, from the chemical evolution point of view, that the BCGs evolve into dSph galaxies after a superwind triggered by several bursts of SF. A more reliable scenario would be the one in which the initial conditions determined the future evolution of these galaxies as proposed by Ferrara & Tolstoy (2000). These authors suggested that some dwarf galaxies might have started their evolution from the same progenitors, but would have followed different evolutionary tracks and that BCGs represent simply a normal tail of the distribution of dwarf galaxies characterized by higher central mass density which favors the onset of occasional starbursts. Some dSph galaxies, instead, could have been formed from protogalactic objects (Pop. III objects - Couchman & Ress 1986, Ferrara 1998, Ciardi, Ferrara & Abel 1999) at very high redshifts ($z_f \sim 15$) and lost their gas content either by blowaway or photoionization.

5 DAMPED LYMAN α SYSTEMS

The Damped Lyman α Systems are the QSO absorption line systems with the highest neutral hydrogen column densities ($N(\text{HI}) \geq 10^{20} \text{ cm}^{-2}$). These systems are believed to be the progenitors of the present day galaxies for several reasons: they dominate the neutral gas content of the universe (Wolfe et al. 1995; Rao & Turnshek 2000), and the comoving mass density of gas inferred from DLAs at $z = 2-3$ is comparable to the current baryonic mass density of stars at the present time (Wolfe et al. 1995; Storrie-Lombardi & Wolfe 2000). As DLAs can be observed at very high redshifts (up to $z \sim 4.4$) they can probe the very early stages of evolution of galactic systems. Thus, the understanding of their nature is a key factor in our knowledge of the formation and evolution of galaxies.

The nature of DLAs at high redshifts, however, is still a matter of debate and several hypothesis have been drawn

recently, including disk galaxies, dwarf irregular galaxies, low surface brightness galaxies (Wolfe et al. 1986; Prochaska & Wolfe 1997, 1998; Pettini et al. 1999; Centurion et al. 2000; Boissier & Prantzos 2000; Molaro et al. 2001). A picture of a multi-population of galaxies being responsible for the absorption seen in DLAs is emerging from studies of possible hosts of DLAs which revealed a wide range of morphological types and luminosities (Lanzetta et al. 1997; Pettini et al. 2000; Turnshek et al. 2001).

Several studies addressing the question of the nature of DLAs from the chemical evolution point of view appeared in the last few years and some connections between the DLAs and dwarf galaxies were suggested by studies using chemical evolution or chemodynamical models compared to a series of abundance ratios observed in DLAs. In a germinal paper Matteucci, Molaro & Vladilo (1997) compared the predictions of chemical evolution models with observed α/Fe and N/α ratios and suggested that starburst galaxies could be the progenitors of some DLAs. More recently, Calura, Matteucci & Vladilo (2003), using chemical evolution models representing galaxies of different morphological types, pointed out that the majority of DLAs can be explained either by disks of spirals observed at large galactocentric distances or by starburst dwarf irregular galaxies and irregular galaxies such as the Large Magellanic Cloud. The dwarf spheroidal were also claimed as possible progenitors for the DLAs by Lanfranchi & Friaça (2003) who used a chemodynamical model. In their simulations, a series of starbursts driven by gas flows inside the galaxy are able to reproduce the majority of the DLAs. In this work, we considered also the BCGs and the dSph galaxies as possible candidates in our attempt to recover the nature of DLAs. The models used are the same as described in the previous sections. For the models of BCGs, though, we used also higher SF efficiencies relative to the standard model in order to account for all the observed systems.

In Figures 12 and 13 the predictions of the standard model for dSph galaxies are compared to $[\text{Si}/\text{Fe}]$ corrected for dust depletion and $[\text{N}/\text{Si}]$ observed in DLAs as a function of metallicity and redshift, respectively. The corrected values of $[\text{Si}/\text{Fe}]$ and $[\text{Fe}/\text{H}]$ are those from the case E00 of Vladilo (2002) and the $[\text{N}/\text{Si}]$ ratios were taken from the compilation of Centurion et al. (2003). The letters correspond to systems where both ratios are available. The appearance of these plots is however misleading and some remarks must be made. In the plot of $[\text{Si}/\text{Fe}]$ and $[\text{N}/\text{Si}]$ as a function of metallicity the dSph model seems to account for almost all the systems, but some of them, especially the ones at high metallicities ($[\text{Si}/\text{H}] > \sim -0.7$), achieve their observed $[\text{N}/\text{Si}]$ ratios only a long time after the onset of the wind. As the wind is very efficient in removing the gas content of the galaxy, it is unlikely that the dSph galaxies could be related to these DLAs, since these objects contain a large amount of gas. In fact, at the highest $[\text{Si}/\text{H}]$ the models predict a HI column density below the ones characteristic of DLAs ($\log N(\text{HI}) \leq 20$ at $[\text{Si}/\text{H}] \geq -0.7$ for the models with $\nu \leq 0.05 \text{ Gyr}^{-1}$). All the other DLAs, however, could be explained as possible progenitors of dSph galaxies since there is a good agreement between the abundance ratios observed in DLAs and the predictions of the dSph model. A more complete comparison, though, could be made with the systems which have both ratios measured. Unfortunately, there are

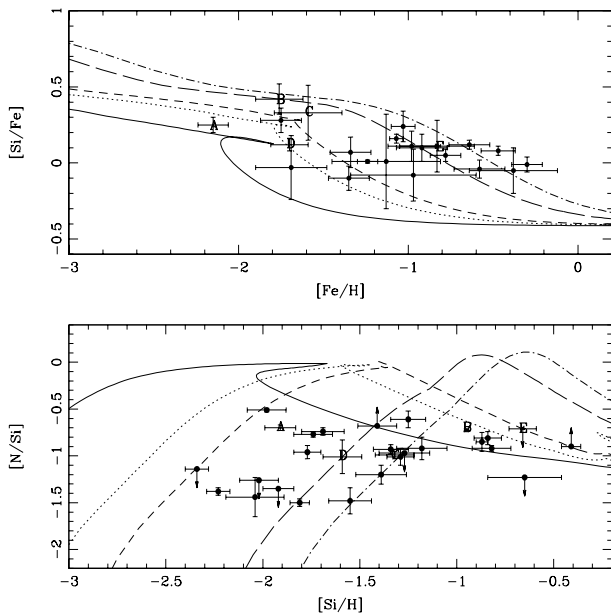


Figure 12. [Si/Fe] vs [Fe/H] corrected for dust (above) and [N/Si] vs [Si/H] (below) observed in DLAs compared to the predictions of the standard model for dSph galaxies with different SF efficiencies (in Gyr^{-1}): 0.01 (solid line), 0.05 (dotted), 0.1 (dashed), 0.5 (long-dashed), 1.0 (dotted-dashed). The letters correspond to DLAs with both ratios observed.

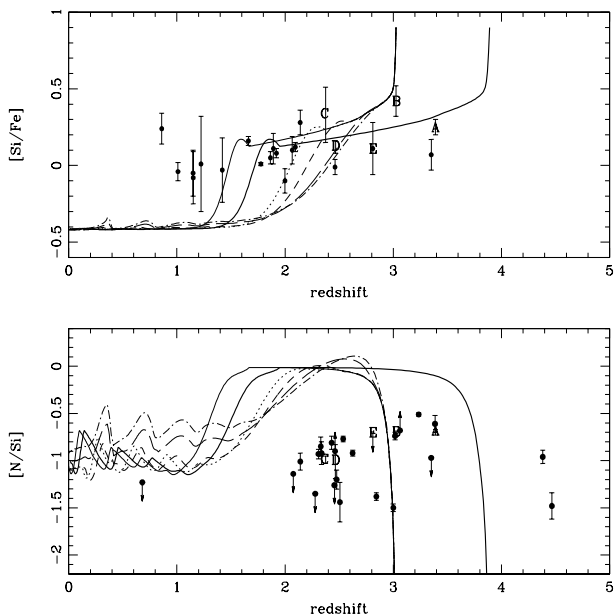


Figure 13. Evolution with redshift of [Si/Fe] corrected for dust (above) and [N/Si] (below) observed in DLAs compared to the predictions of the standard model for dSph galaxies with different SF efficiencies (in Gyr^{-1}) assuming a formation redshift 5 (thin lines). It is also shown a model with formation redshift $z_f = 8$ and $\nu = 0.1 Gyr^{-1}$ (thick line). The other lines are the same as in Figure 12. The letters correspond to DLAs with both ratios observed.

only 5 systems with simultaneous [Si/Fe] and [N/Si] (letters A to E in Figures 12 and 13) and no accurate conclusions can be reached. Only 2 out of 5 systems (B and C) seems to be reproduced by the models with the same SF efficiency and at the same epoch. The other systems (A, D and E) require either a different SF efficiency or different epochs of burst occurrence to reproduce each abundance ratio. In the diagram of abundance ratios as a function of redshift, on the other hand, the lack of agreement between the predictions of the dSph models and the observed data does not mean that a scenario where the DLAs become dSph galaxies should be discarded. For the sake of simplicity we assumed the same formation redshift for all systems, and this could be unrealistic. Each DLA could have been formed at a different cosmic epoch and have followed a different evolutionary track. Therefore, this diagram shows that, if the dSph galaxies are the progenitors of the DLAs, one is seeing the earliest stages of evolution of these systems before or at the onset of the wind and that the dSph galaxies would be seen as a DLAs only during a well defined period of time, no longer than 4 Gyr. After that time, their HI column densities fall below the limit which characterizes the DLAs. A point which plays against the scenario in which the DLAs would be the progenitors of the local dSph galaxies is the differences in the abundance patterns of Zn observed in DLAs and in dSph galaxies, respectively. In the dSph galaxies of the Local Group, the observed Zn/Fe is always below solar (Shetrone, Cotè & Sargent 2001) whereas even in the less dusty DLAs this ratio is above solar. This fact might indicate that the DLAs are in fact not related to dSph galaxies or that the evolution with time of Fe and Zn are different or even that different amounts of Zn and Fe are lost in the galactic wind. Unfortunately, the nucleosynthesis of Zn is not fully understood and no firm conclusions can be drawn.

The case of the BCGs is more promising. In Figures 14 and 15, respectively, the predictions of the standard model with 7 bursts for BCGs compared to the observed [Si/Fe] (corrected for dust) and [N/Si] as a function of metallicity and redshift are shown, respectively. In all cases the models can account for all the observed systems, if higher SF efficiencies are adopted. While the data of BCGs require a SF efficiency in the range $\nu = 0.1 - 0.9 Gyr^{-1}$, the abundance ratios in DLAs are fully reproduced by the standard model for BCGs with ν in the range $\nu = 0.3 - 2.5 Gyr^{-1}$. In this case, the DLAs with both abundance ratios measured are reproduced by the same models at the same time with the exception of system E, which is not reproduced even by the dSph model. In the BCGs scenario, contrary to the dSphs, only one formation redshift ($z_f = 5$) is necessary to reproduce the data at all epochs suggesting that the DLAs could have started forming stars at the same cosmic epoch and, be observed at different stages of evolution.

Two remaining problems, though, are the high values for the predictions of [N/Si] and the claimed bimodal distribution of DLAs (Prochaska et al. 2002; Centurion et al. 2003). We adopted two alternative scenarios in the BCGs model in order to try to explain these features. First we considered a top-heavy IMF with an exponent $x=0.1$, as suggested by Prochaska et al. (2002) and Henry & Prochaska (2003). Indeed, if a top-heavy IMF is assumed the models predict very low values for [N/Si], but, at the same time, very high [Si/Fe] ratios, well above all systems observed (Figure

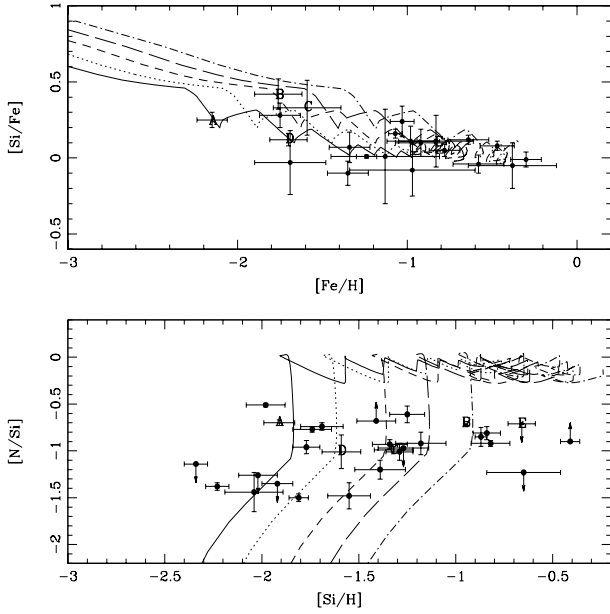


Figure 14. $[\text{Si}/\text{Fe}]$ vs $[\text{Fe}/\text{H}]$ corrected for dust (above) and $[\text{N}/\text{Si}]$ vs $[\text{Si}/\text{H}]$ (below) observed in DLAs compared to the predictions of the standard model for BCGs with 7 bursts with different SF efficiencies (in Gyr^{-1}): 0.3 (solid line), 0.5 (dotted), 0.9 (dashed), 1.5 (long-dashed), 2.5 (dotted-dashed). The letters correspond to DLAs with both ratios observed.

16), making clear that a top-heavy IMF cannot explain the low values found for some DLAs. Another possibility would be the model for BCGs with 4 bursts, since it predicts low values of N/O during the third burst. We used this model and included primary production of N in massive stars in order to try to explain the plateau at low values of $[\text{N}/\alpha]$ suggested by Prochaska et al. (2002) and Centurion et al. (2003). If a very low amount of primary N, roughly in agreement with the yields of the model with $Z=0.004$ of Meynet & Maeder (2002), is assumed to be produced in massive stars, then the models reproduce the N/O distribution of BCGs (Figure 10) and predict a plateau at the same values observed in low-N DLAs (Figure 17). This plateau, in the models, is a result of a very short burst (20 Myr) of SF at the very early stages of the evolution combined with the assumed low level of primary production of N in massive stars. During the burst both α elements and N are produced in massive stars and injected into the ISM giving rise to a constant N/ α ratio, which has a low value due to the short burst duration and to the low amount of primary N produced. It should be mentioned, however, that the suggested bimodal distribution, characterized by this plateau at low values of $[\text{N}/\alpha]$, could not be real and should be confirmed by more data, and that the production of primary N in massive stars, although predicted by stellar models with rotation (Meynet & Maeder 2002), is not necessarily required to explain the N/O ratio observed in different environments (Chiappini, Romano & Matteucci 2003).

6 SUMMARY

We analysed the star formation and chemical evolution both in dSph galaxies of the Local Group and in BCGs compar-

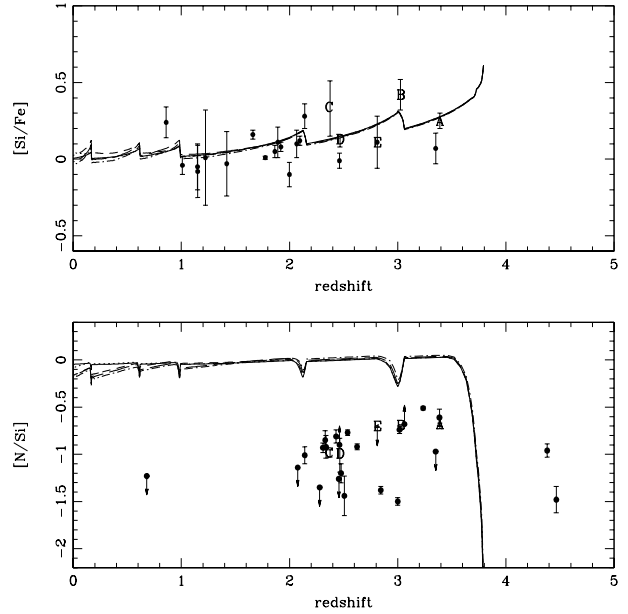


Figure 15. Evolution with redshift of $[\text{Si}/\text{Fe}]$ corrected for dust (above) and $[\text{N}/\text{Si}]$ (below) observed in DLAs compared to the predictions of the standard model for BCGs with 7 bursts with different SF efficiencies (in Gyr^{-1}) assuming a formation redshift 5. The lines are the same as in Figure 14. The letters correspond to DLAs with both ratios observed.

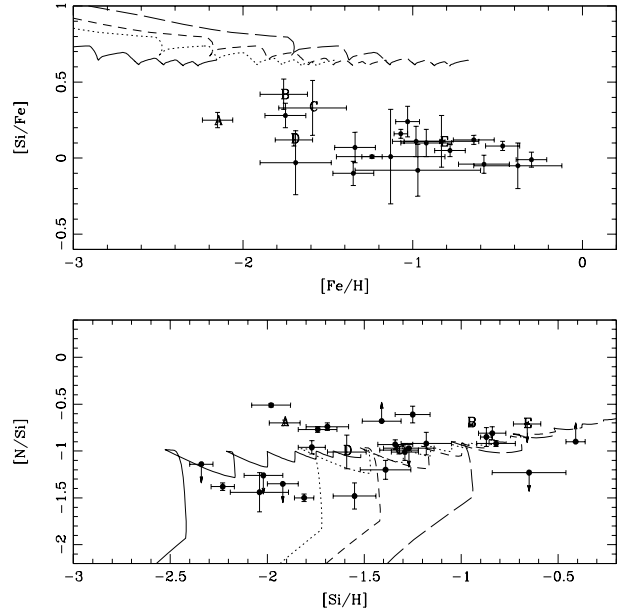


Figure 16. $[\text{Si}/\text{Fe}]$ vs $[\text{Fe}/\text{H}]$ (above) corrected for dust and $[\text{N}/\text{Si}]$ vs $[\text{Si}/\text{H}]$ (below) observed in DLAs compared to the predictions of the standard model for BCGs assuming a IMF with an exponent $x=0.1$. The lines represent different SF efficiencies (in Gyr^{-1}): 0.01 (solid line), 0.05 (dotted), 0.1 (dashed), 0.3 (long-dashed). The letters correspond to DLAs with both ratios observed.

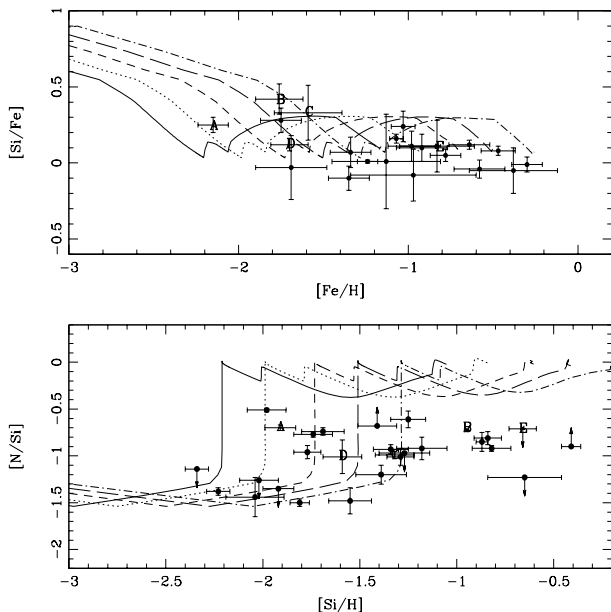


Figure 17. $[\text{Si}/\text{Fe}]$ vs $[\text{Fe}/\text{H}]$ (above) corrected for dust and $[\text{N}/\text{Si}]$ vs $[\text{Si}/\text{H}]$ (below) observed in DLAs compared to the predictions of the standard model for BCGs with 4 bursts assuming a primary production of N in massive stars. The lines represent different SF efficiencies (in Gyr^{-1}): 0.3 (solid line), 0.5 (dotted), 0.9 (dashed), 1.5 (long-dashed), 2.5 (dotted-dashed). The letters correspond to DLAs with both ratios observed.

ing several observed abundance ratios to the predictions of detailed chemical evolution models. By taking into account the role played by supernovae of different types (II, Ia) and adopting up to date nucleosynthesis prescriptions we followed the evolution of several chemical elements (H, D, He, C, N, O, Mg, Si, S, Ca, and Fe). Each galaxy model was specified by the prescriptions of the SF and wind efficiency in the sense that one long episode of star formation and a high wind efficiency characterize the dSph galaxies, whereas the BCGs are represented by SF occurring in several short bursts separated by long quiescent periods and a low wind efficiency. The predictions of the models were compared with the $[\alpha/\text{Fe}]$ ratios in dSph galaxies and with C/O, N/O, Si/O and with $[\text{O}/\text{Fe}]$ in BCGs. A possible connection between these two types of galaxies in a unified evolutionary scenario as well as the hypothesis that the dSph galaxies or BCGs could be related to DLAs were also analysed.

The main conclusions can be summarized as follows:

- by adopting a standard model for the sample of 8 dSph galaxies of the Local Group, the observed $[\alpha/\text{Fe}]$ ratios are reproduced with a SF occurring in 1 long burst lasting 8 Gyr, with an efficiency of SF in the range $\nu = 0.01 - 1.0 \text{ Gyr}^{-1}$;
- each galaxy with enough data is also reproduced by a model following the main prescriptions of the standard model, but with the number, epoch and duration of the bursts as suggested by the SF histories inferred by CMDs. The differences in the abundance patterns of each galaxy are mainly due to different efficiencies in the star formation rate rather than to details in the histories of SF;
- a very efficient galactic wind ($w_i \sim 5 - 15$, depending on the SF efficiency) is required to reproduce the gas content, total mass and abundance ratios observed in local

dSph galaxies. The low gas content of the dSph galaxies is the result of the consumption of gas by the SF coupled with gas removal by galactic winds;

- the N/O, C/O, Si/O and $[\text{O}/\text{Fe}]$ ratios observed in BCGs can be explained by a model with 2 to 7 short bursts of SF with efficiencies in the range $\nu = 0.1 - 0.9 \text{ Gyr}^{-1}$;
- the low values of N/O at low O/H observed in BCGs could be the natural result of a model with 4 bursts of SF where the first one occurs at early galactic ages and the others at more recent times. In such a scenario, there is no need of invoking primary production of N in massive stars, even though the adoption of low amounts of primary N in these stars does not change much the results;
- a Salpeter (1955) IMF seems to reproduce at best the properties of both dSph galaxies and BCGs;
- a connection between dSph galaxies and BCGs in a unified evolutionary scenario is not likely, owing to the large differences in the chemical evolution history of these galaxies;

• the dSph and BCG models suggest two different possible pictures for the DLAs: while the BCG models can reproduce all observed DLAs at all epochs and suggest that these systems could have been formed at the same cosmic epoch (around $z_f = 5$) but observed at different stages of their evolution, only the DLAs with low metallicities ($[\text{Si}/\text{H}] \leq -0.7$) could be related to dSph galaxies and, in this case, they should be very young systems which have been formed within a wide range of redshifts;

• the suggested plateau at low N/α observed in DLAs can possibly be explained by the model for BCGs with 4 bursts of SF if a low level of primary N produced in massive stars is adopted. In this case, the plateau should be the result of a very short (20 Myr) initial starburst when both α -elements and N would be produced by massive stars. As the burst is short and the amount of primary N is low, the predicted value of the N/α ratio would be also low. The predicted α/Fe ratios, however, would be very high ($[\alpha/\text{Fe}] \geq 0.5$), above all the observed values and at metallicities well below the ones seen in DLAs ($[\text{Fe}/\text{H}] \leq -2.3$). Consequently, if this scenario is the explanation for the suggested plateau, then one should observe such low Fe abundances and high α/Fe ratios in the DLAs which have low N/α (~ -1.6 dex). Another uncertainty concerning the plateau predicted by the models is the adopted amount of primary N produced in massive stars. Our value is roughly in agreement with the model with $Z=0.004$ of Meynet & Maeder (2002), but only the BCG model with the highest SF efficiency reaches this metallicity. For all the other models, the amount of primary N produced by massive stars would be lower (as in the model with $Z=10^{-5}$ of Meynet & Maeder 2002) and consequently the predicted N/α would lie below the observed plateau. Therefore, in this case, the primary N produced by massive stars, as suggested by the yields of Meynet & Maeder (2002), could not be the explanation for the observed plateau, if this plateau is real.

ACKNOWLEDGMENTS

We thank C. Chiappini, F. Calura, S. Recchi for many useful discussions. G.A.L. also thanks the hospitality of the Dipartimento di Astronomia-Università di Trieste and of the

Astronomical Observatory of Trieste which provided all the support during his stay. G.A.L. acknowledges financial support from the Brazilian agency FAPESP (proj. 00/10972-0).

REFERENCES

- Arimoto N., Yoshii Y., 1987, *A&A*, 173, 23
 Boissier S., Prantzos N., 2000, *MNRAS*, 312, 398
 Bonifacio P., Hill V., Molaro P., Pasquini L., Di Marcantonio P., Santin P., 2000, *A&A*, 359, 663
 Bradamante F., Matteucci F., D’Ercole A., 1998, *A&A*, 337, 338
 Calura F., Matteucci F., Vladilo G., 2003, *MNRAS*, 340, 59
 Carigi L., Colin P., Peimbert M., Sarmiento A., 1995, *ApJ*, 445, 98
 Carigi L., Hernandez X., Gilmore G., 2002, *MNRAS*, 334, 117
 Carraro G., Chiosi C., Girardi L., Lia C., 2001, *MNRAS*, 327, 69
 Centurión M., Bonifacio P., Molaro P., Vladilo G., 2000, *ApJ*, 536, 540
 Centurión M., Molaro P., Vladilo G., Peroux C., Levshakov S.A., D’Odorico V., 2003, *A&A*, 403, 55
 Chiappini C., Romano D., Matteucci F., 2003, *MNRAS*, 339, 63
 Ciardi B., Ferrara A., Abel T., 1999, *ApJ*, 533, 594
 Couchman H.M.P., Rees M.J., 1986, *MNRAS*, 221, 53
 Davies J.I., Phillipps S., 1988, *MNRAS*, 233, 553
 Dekel A., Silk J., 1986, *ApJ*, 303, 39
 D’Ercole A., Brighenti F., 1999, *MNRAS*, 309, 941
 Dolphin A.E., 2002, *MNRAS*, 332, 91
 Doublier V., Comte G., Petrosian A., Surace C., Turatto M., 1997, *A&AS*, 124, 405
 Doublier V., Kunth D., Courbin F., Magain P., 2000, *A&A*, 353, 887
 Ferrara A., 1998, *ApJ*, 499, L17
 Ferrara A., Tolstoy E., 2000, *MNRAS*, 313, 291
 Garnett D.R., Skillman E.D., Dufour R.J., Peimbert M., Torres-Peimbert S., Terlevich R., Terlevich E., Shields G.A., 1995, *ApJ*, 443, 64
 Garnett D.R., Skillman E.D., Dufour R.J., Shields G.A., 1997, *ApJ*, 481, 174
 Grevesse N., Sauval A.J., 1998, *Space Science Reviews*, 85, 161
 Hernandez X., Gilmore G., Valls-Gabaud D., 2000, *MNRAS*, 317, 831
 Ikuta C., Arimoto, N., 2002, *A&A*, 391, 55
 Izotov Y.I., Thuan T.X., 1999, *ApJ*, 511, 639
 Kobulnicky H.A., Skillman E.D., 1996, *ApJ*, 471, 211
 Kunth D., Ostlin G., 2000, *A&AR*, 10, 1
 Kunth D., Matteucci F., Marconi G., 1995, *A&A*, 297, 634
 Lanfranchi G., Friaça A.C.S., 2003, accepted *MNRAS*, astro-ph/0304119
 Lanzetta K.M., Wolfe A.M., Altan H., Barcons X., Chen H.W., Fernández-Soto A., Meyer D.M., Ortiz-Gil A., Savaglio S., Webb J.K., Yahata N., 1997, *AJ*, 114, 1337
 Larsen T.I., Sommer-Larsen J., Pagel B.E.J., 2001, *MNRAS*, 322, 555
 Lin D.N.C., Faber S.M., 1983, *ApJ*, 266L, 21
 Marconi G., Matteucci F., Tosi M., 1994, *MNRAS*, 270, 35
 Marlowe A.T., Meurer G.R., Heckman T.M., 1999, *ApJ*, 522, 183
 Mateo M.L., 1998, *ARA&A*, 36, 435
 Matteucci F., 1986, *MNRAS*, 221, 911
 Matteucci F., 1992, *ApJ*, 397, 32
 Matteucci F., Chiosi C., 1983, *A&A*, 123, 121
 Matteucci F., Tornambé A., 1987, *A&A*, 185, 51
 Matteucci F., Tosi M., 1985, *MNRAS*, 217, 391
 Matteucci F., Molaro P., Vladilo G., 1997, *A&A*, 321, 45
 Meynet G., Maeder A., 2002, *A&A*, 390, 561
 McLow M., Ferrara A., 1999, *ApJ*, 513, 142
 Molaro P., Levshakov S.A., D’Odorico S., Bonifacio P., Centurión M., 2001, *ApJ*, 549, 90
 Nomoto K., Hashimoto M., Tsujimoto T., Thielemann F.-K., Kishimoto N., Kubo Y., Nakasato N., 1997, *Nucl. Phys. A*, 616, 79c
 Papaderos P., Loose H.-H., Fricke K.J., Thuan T.X., 1996a, *A&A*, 314, 59
 Papaderos P., Loose H.-H., Thuan T.X., Fricke K.J., 1996b, *A&AS*, 120, 207
 Pettini M., Ellison S.L., Steidel C.C., Bowen D.V., 1999, *ApJ*, 510, 576
 Pettini M., Ellison S.L., Steidel C.C., Shapley A. E., Bowen D.V., 2000, *ApJ*, 532, 65
 Pilyugin L.S., 1993, *A&A*, 277, 42
 Prochaska J.X., Wolfe A.M., 1997, *ApJ*, 474, 140
 Prochaska J.X., Wolfe A.M., 1998, *ApJ*, 507, 113
 Prochaska J.X., Henry R.B.C., O’Meara J.M., Tytler D., Wolfe A.M., Kirkman D., Lubin D., Suzuki N., 2002, *PASP*, 114, 933
 Prochaska J.X., Henry R.B.C., 2003, in *CNO in the Universe*, ASP Conference Series, ed Charbonnel C., Schaerer D., and Meynet G., in press, astor-ph/0211512
 Rao S.M., Turnshek D.A., 2000, *ApJS*, 130, 1
 Recchi S., Matteucci F., D’Ercole A., 2001, *MNRAS*, 322, 800
 Recchi S., Matteucci F., D’Ercole A., Tosi M., 2002, *A&A*, 384, 799
 Salpeter E.E., 1955, *ApJ*, 121, 161
 Scalo J.M., 1986, *FCPh*, 11, 1
 Smecker-Hane T., 1997, in *Star Formation Near and Far*, Seventh Astrophysics Conference at College Park Maryland, ed S.S. Holt and L.G. Mund (AIP Press, New York), p.571
 Smecker-Hane T., Mc William A., 1999, in Hubeny I. et al., eds. *Spectrophotometric Dating of Stars and Galaxies*, ASP Conference Proceedings, Vol. 192, p.150
 Shetrone M.D., Bolte M., Stetson P.B., 1998, *AJ*, 115, 1888
 Shetrone M., Côté P., Sargent W.L.W., 2001, *ApJ*, 548, 592
 Shetrone M., Venn K.A., Tolstoy E., Primas F., 2003, *AJ*, 125, 684
 Silk J., 2002, astro-ph/0212068
 Storrie-Lombardi L.J., Wolfe A.M., 2000, *ApJ*, 543, 552
 Thielemann F.K., Nomoto K., Hashimoto M., 1996, *ApJ*, 460, 408
 Tolstoy E., Venn K.A., Shetrone M., Primas F., Hill V., Kaufer A., Szeifert T., 2003, *AJ*, 125, 707
 Turnshek D.A. Rao S., Nestor D., Lane W., Monier E., Bergeron J., Smette A., 2001, *ApJ*, 553, 288
 Vader J.P., 1986, *ApJ*, 305, 669
 van den Bergh S., 1994, *ApJ*, 428, 617
 Van den Hoeck L.B., Groenewegen M.A.T., 1997, *A&AS*, 123, 305
 Vladilo G., 2002, *A&A*, 391, 407
 Wolfe A.M., Turnshek D.A., Smith H.E., Cohen R.D., 1986, *ApJS*, 61, 249
 Wolfe A.M., Lanzetta K.M., Foltz C.B., Chaffee F.H., 1995, *ApJ*, 454, 698
 Woosley S.E., Weaver, T.A., 1995, *ApJS*, 101, 181

This paper has been produced using the Royal Astronomical Society/Blackwell Science \LaTeX style file.